Rheologica Acta (2021) 60:11–21
https://doi.org/10.1007/s00397-020-01248-y

ORIGINAL CONTRIBUTION

Effective viscosity and Reynolds number of non-Newtonian fluids using Meter model

Takshak Shende[1] · Vahid J. Niasar[1] · Masoud Babaei[1]

Received: 22 May 2020 / Revised: 30 September 2020 / Accepted: 3 October 2020 / Published online: 10 November 2020

Abstract

The Meter model (a four-parameter model) captures shear viscosity–shear stress relationship (S-shaped type) of polymeric non-Newtonian fluids. We devise an analytical solution for radial velocity profile, average velocity, and volumetric flow rate of steady-state laminar flow of non-Newtonian Meter model fluids through a circular geometry. The analytical solution converts to the Hagen–Posseuille equation for the Newtonian fluid case. We also develop the formulations to determine effective viscosity, Reynolds number, and Darcy's friction factor using measurable parameters as available rheological models do not correctly define these parameters for a given set of flow condition in circular geometry. The analytical solution and formulations are validated against experimental data. The results suggest that the effective Reynolds number and effective friction factor estimated using the proposed formulation help characterize non-Newtonian fluid flow through a circular geometry in laminar and turbulent flows.

Keywords Non-Newtonian fluid · Shear stress · Viscosity · Analytical solution · Shear-thinning fluid · Reynolds number · Micro-capillary fluid flow

Introduction

The laminar flow of a non-Newtonian fluid (described using generalized Newtonian fluid model) through a circular capillary/tube has broader engineering application (e.g., polymer fluid flow through pipes in industrial settings (Bird et al. 1987), capillary bundle model of porous media (Savins 1969), pore-network model (Sochi and Blunt 2008)). Among generalized Newtonian fluid models (Yilmaz and Gundogdu 2008), Cross (Cross 1965), Carreau (Yasuda 1979), Carreau–Yasuda (Yasuda 1979), Meter (Meter and Bird 1964; Meter 1964; Savins 1969; Tsakiroglou 2002; Tsakiroglou et al. 2003; Tsakiroglou et al. 2003), and Steller–Ivako (Steller and Iwko 2018) models can predict S-shaped rheological properties (i.e., constant viscosity at low and high shear values and decreasing viscosity at intermediate shear values) of many shear-thinning fluids.

Attempts have been made by many investigators to obtain an analytical solution for flow of non-Newtonian fluid through a circular tube. Matsuhisa and Bird derived an analytical solution for the laminar flow of a fluid obeying shear stress–dependent Ellis model (Matsuhisa and Bird 1965). Meter and Bird proposed the analytical solution for the flow of shear stress–dependent Meter model fluid in a circular capillary if $\frac{\eta_\infty}{\eta_0}$ is very small. Here, η_0 and η_∞ are zero and infinite shear viscosity, respectively (Meter and Bird 1964). Although Sochi (2015) and Kim (2018) proposed analytical solutions for Carreau and Cross fluid flow through a circular tube and Peralta et al. (2014, 2017) proposed analytical solution for flow over free-draining vertical plate, the exact analytical solution is absent for estimation of the radial velocity profile, average velocity, and volumetric flow rate of fluid flow in a circular tube/micro-capillary obeying Cross, Carreau, Meter, or Steller–Ivako model.

The Reynolds number of non-Newtonian fluids in a circular tube/capillary is commonly defined using the viscosity of the fluid at the wall (Escudier et al. 2005;

Electronic supplementary material The online version of this article (https://doi.org/10.1007/s00397-020-01248-y) contains supplementary material, which is available to authorized users.

✉ Masoud Babaei
masoud.babaei@manchester.ac.uk

[1] Department of Chemical Engineering and Analytical Science, The University of Manchester, Manchester, UK

Kim 2018), the zero-shear viscosity (Ferrás et al. 2020), or Metzner and Reeds equation (Metzner and Reed 1955). The shear viscosity of non-Newtonian fluids varies along the radial direction in a fully developed circular capillary. Thus, zero shear viscosity or the viscosity of the fluid at the wall is not the representative viscosity or the effective viscosity of fluid flow. Metzner and Reeds equation is applicable for purely power-law fluid.

The effective viscosity of the fluid is analogous to the average velocity of the fluid. Both vary spatially during fluid flow in the circular capillary. Thus, similar to the average velocity value, the effective viscosity value is a single representative viscosity value for fluid flow under a given set of conditions. Sadowski and Bird (1965) defined the effective viscosity of the Ellis model fluid, as in Eq. 1, based on the exact analytical solution for the flow of the Ellis model fluid in the circular capillary:

$$\frac{1}{\eta_{\mathrm{eff}}} = \frac{1}{\eta_0}\left(1 + \frac{4}{\alpha+3}\left(\frac{\tau_{\mathrm{w}}}{\tau_{\frac{1}{2}}}\right)^{\alpha-1}\right) \tag{1}$$

here, η_{eff} is the effective viscosity of the fluid, η_0 is the zero shear viscosity, α is an exponent, $\tau_{\frac{1}{2}}$ is the critical shear stress parameter, and τ_{w} is the wall shear stress. The effective viscosity helps define the Reynolds number and Darcy's friction factor. Furthermore, effective viscosity helps upscale shear viscosity from pore scale to Darcy scale (Savins 1969; Sadowski and Bird 1965; Balhoff and Thompson 2006; Duda et al. 1983; Eberhard et al. 2019) during the flow of polymeric fluid in the porous media. Effective viscosity and the exact analytical solution are useful in developing pore-network models for the flow of non-Newtonian fluids in porous media (Sochi and Blunt 2008). The pore-network model for non-Newtonian fluid has wider engineering and industrial applications, e.g., it helps understand the complex interaction of the non-Newtonian fluids with tortuous and heterogeneous porous media at pore scale.

A formulation to define an effective viscosity (η_{eff}) of non-Newtonian fluids (having S-shaped type rheology) for a given flow condition using measurable parameters is absent in the literature. Absence of an analytical solution to estimate the average velocity of Cross and Carreau fluid makes correlating Reynolds number with Darcy's friction factor arduous.

To address the above discrepancy, we obtain an exact analytical solution for flow of a Meter model fluid through circular geometry. The analytical solution of the Meter model (MM) helps define effective viscosity, Reynolds number, and friction factor of non-Newtonian fluid flow using measurable parameters.

Mathematical formulation

The Cauchy momentum equation describes momentum transfer in any continuum. The state of stress at any point in the continuum (i.e., normal stresses, σ_n, and shear stresses, τ) is defined using Cauchy's stress tensor ($\boldsymbol{\sigma}$). For an incompressible fluid, divergence of Cauchy's stress tensor is $\nabla\cdot\boldsymbol{\sigma} = -\nabla P + \nabla\cdot\boldsymbol{\tau}$, where ∇P is the pressure gradient and $\boldsymbol{\tau}$ is the deviatoric stress tensor. The constitutive equation of generalized Newtonian fluid (GNF) defines viscosity of the fluid as a non-linear function of second invariant of either rate-of-deformation tensor (i.e., $\boldsymbol{\tau} = 2\,\eta(\dot{\gamma})\,\boldsymbol{D}$) (Bird et al. 2007) or deviatoric stress tensor (i.e., $\boldsymbol{\tau} = 2\,\eta(\tau)\,\boldsymbol{D}$) (Meter and Bird 1964; Steller and Iwko 2018; Peters et al. 1999; Matsuhisa and Bird 1965). Here, $\boldsymbol{D} = \frac{1}{2}\dot{\boldsymbol{\gamma}} = \frac{1}{2}(\nabla\mathbf{u} + (\nabla\mathbf{u})^T)$, the magnitude of shear rate is $|\dot{\gamma}| = \sqrt{\dfrac{\dot{\boldsymbol{\gamma}}:\dot{\boldsymbol{\gamma}}}{2}}$ (Bird et al. 2007), the magnitude of shear stress is $|\tau| = \sqrt{\dfrac{\boldsymbol{\tau}:\boldsymbol{\tau}}{2}}$ (Meter and Bird 1964), and $\mathbf{u}$ is velocity vector. The constitutive equations for commonly used shear rate–dependent and shear stress–dependent GNF models are given in Table S1 of the Supporting Information (SI).

The intermolecular and interparticle interactions in the fluid generate stresses (i.e., normal and shear stresses). These stresses govern the flow properties of the non-Newtonian fluids, including the viscosity of fluids. Thus, the stress-based model shall be adopted to describe the physics behind non-Newtonian fluid flow through void spaces. Meter (Meter and Bird 1964) proposed his model in 1964 to describe S-shaped type rheology of a non-Newtonian fluid. The Meter model is a modified version of the Ellis model (Bird and Carreau 1968), and Reiner-Philippoff model (Reiner 1930; Philippoff 1935) which were independently proposed in 1927, 1930, and 1935, respectively; thus, it could also be renamed as the truncated Ellis-Reiner-Philippoff model.

The Meter model (Eq. 2) gives viscosity of a non-Newtonian fluid in terms of shear stress as follows (Meter and Bird 1964):

$$\eta = \eta_\infty + \frac{\eta_0 - \eta_\infty}{1 + \left(\dfrac{\tau}{\tau_{\mathrm{m}}}\right)^{\alpha-1}} \tag{2}$$

here, η (Pa·s) is the shear viscosity at a given shear stress (τ); η_0 (Pa·s) is the viscosity at the zero shear stress (i.e., zero shear viscosity); η_∞ (Pa·s) is the viscosity at the infinite shear stress (i.e., infinite shear viscosity); τ_{m} (Pa) is the critical shear stress of the non-Newtonian fluid at which viscosity of the solution drops to $\frac{\eta_0+\eta_\infty}{2}$; α is the shear stress-dependent exponent of the Meter model. η_0,

η_∞, and τ_m are measurable quantities of the non-Newtonian fluid. Here, we slightly modify the denotation of the Meter model by replacing $\alpha - 1$ with S; where, S is the shear stress-dependent exponent of the Meter model (MM). The characteristic time (λ) of the MM (Eq. 3) is a time at which fluid transition from Newtonian behavior (zero shear viscosity) to shear thinning or shear thickening behavior (i.e., at τ_m) occurs.

$$\lambda = \frac{\eta_0 + \eta_\infty}{2\,\tau_m} \tag{3}$$

The shear rate of MM is

$$\dot{\gamma} = \frac{\tau}{\eta_\infty + \frac{\eta_0 - \eta_\infty}{1 + \left(\frac{\tau}{\tau_m}\right)^S}} \tag{4}$$

We note that Eq. 4 applies to the Newtonian fluid (if $\eta_0 = \eta_\infty$, $S = 1$, $\tau_m = 1$), shear-thinning fluid (if $\eta_0 > \eta_\infty$, $S > 0$, $\tau_m > 0$), and shear-thickening fluid (if $\eta_0 < \eta_\infty$, $S > 0$, $\tau_m > 0$).

Analytical solution

Adopting Hagen-Poiseuille framework, the analytical solution is derived for a fully developed, incompressible, isothermal, laminar, steady, unidirectional flow of shear stress-dependent time-independent non-Newtonian fluid through a circular tube of radius (R) under constant pressure gradient of $\left(\frac{dP}{dx}\right)$.

The shear rate $\dot{\gamma}(r)$ along radial direction r is defined as:

$$\dot{\gamma}(r) = \frac{\tau}{\eta}, \tag{5}$$

Substituting Eq. 2 in Eq. 5, we obtain:

$$\dot{\gamma}(r) = \frac{\tau}{\eta_\infty + \dfrac{\eta_0 - \eta_\infty}{1 + \left(\dfrac{\tau}{\tau_m}\right)^S}}, \tag{6}$$

The shear rate $\dot{\gamma}(r)$ in terms of velocity $u(r)$ along radial position r is as defined in Eq. 7:

$$\dot{\gamma}(r) = -\frac{du(r)}{dr}, \tag{7}$$

The shear stress (τ) in a circular tube under a constant pressure gradient of $\frac{dP}{dx}$ in x-direction is as defined in Eq. 8:

$$\tau = -\frac{dP}{dx}\frac{r}{2}, \tag{8}$$

Now, substituting Eq. 7 and Eq. 8 in Eq. 6, we obtain:

$$-\frac{du(r)}{dr} = \frac{\left(-\frac{dP}{dx}\frac{r}{2}\right)}{\eta_\infty + \dfrac{\eta_0 - \eta_\infty}{1 + \left(-\dfrac{dP}{dx}\dfrac{r}{2\,\tau_m}\right)^S}}, \tag{9}$$

The velocity profile along the radial direction can be obtained as follows by integrating Eq. 9:

$$u(r) = \frac{dP}{dx}\frac{r^2}{4\,\eta_0\,\eta_\infty}\Bigg(\eta_0 + (\eta_\infty - \eta_0)_2\mathrm{F}_1 \left(1, \frac{2}{S}; \frac{S+2}{S}; -\frac{\eta_\infty}{\eta_0}\left(-\frac{dP}{dx}\frac{r}{2\,\tau_m}\right)^S\right)\Bigg) + \text{Constant}, \tag{10}$$

here, ${}_2F_1$ is the hypergeometric function as defined in Eq. 17. At the wall of a circular tube, i.e., at $r = R$, by imposing the no-slip boundary condition, $u(R) = 0$, Eq. 10 becomes:

$$\text{Constant} = -\frac{dP}{dx}\frac{R^2}{4\,\eta_0\,\eta_\infty}\Bigg(\eta_0 + (\eta_\infty - \eta_0)_2\mathrm{F}_1 \left(1, \frac{2}{S}; \frac{S+2}{S}; -\frac{\eta_\infty}{\eta_0}\left(-\frac{dP}{dx}\frac{R}{2\,\tau_m}\right)^S\right)\Bigg), \tag{11}$$

Substituting Eq. 11 in Eq. 10, we obtain velocity profile in a circular tube for the Meter model fluid as:

$$\begin{aligned} u(r) = -\frac{dP}{dx}\frac{1}{4\,\eta_0\,\eta_\infty}\Bigg[&R^2\,\Bigg(\eta_0 + (\eta_\infty - \eta_0)_2\mathrm{F}_1 \\ &\times\left(1, \frac{2}{S}; \frac{S+2}{S}; -\frac{\eta_\infty}{\eta_0}\left(-\frac{dP}{dx}\frac{R}{2\,\tau_m}\right)^S\right)\Bigg) \\ &-r^2\Bigg(\eta_0 + (\eta_\infty - \eta_0)_2\mathrm{F}_1\Bigg(1, \frac{2}{S}; \frac{S+2}{S}; -\frac{\eta_\infty}{\eta_0} \\ &\times\left(-\frac{dP}{dx}\frac{r}{2\,\tau_m}\right)^S\Bigg)\Bigg)\Bigg], \end{aligned} \tag{12}$$

The maximum velocity of the Meter model fluid in a circular tube will be at the center of the tube. On substituting $r = 0$ in Eq 12, we obtain maximum velocity as follows:

$$U_{\max} = -\frac{dP}{dx}\frac{R^2}{4\,\eta_0\,\eta_\infty}\Bigg(\eta_0 + (\eta_\infty - \eta_0)_2\mathrm{F}_1 \left(1, \frac{2}{S}; \frac{S+2}{S}; -\frac{\eta_\infty}{\eta_0}\left(-\frac{dP}{dx}\frac{R}{2\,\tau_m}\right)^S\right)\Bigg), \tag{13}$$

Considering Q as the volumetric flow rate, the average velocity in a circular tube is given by:

$$U_{\text{avg}} = \frac{Q}{\pi R^2} = \frac{1}{\pi R^2}\int_0^R 2\pi\, r\, u(r)\, dr, \tag{14}$$

Substituting Eq. 12 in Eq. 14, and integration and simplification, we obtain average velocity during flow of a non-Newtonian Meter model fluid as:

$$U_{\mathrm{avg}} = -\frac{dP}{dx}\frac{R^2}{8\,\eta_0\,\eta_\infty}\Bigg((\eta_\infty-\eta_0)_3\mathrm{F}_2\left(1,\frac{2}{S},\frac{4}{S};\frac{S+2}{S},\frac{S+4}{S};-\frac{\eta_\infty}{\eta_0}\left(-\frac{dP}{dx}\frac{R}{2\,\tau_{\mathrm{m}}}\right)^S\right)+2\,(\eta_0-\eta_\infty)_2\mathrm{F}_1\left(1,\frac{2}{S};\frac{S+2}{S};-\frac{\eta_\infty}{\eta_0}\left(-\frac{dP}{dx}\frac{R}{2\,\tau_{\mathrm{m}}}\right)^S\right)-\eta_0\Bigg), \tag{15}$$

The analytical solution to estimate the volumetric flow rate (Q) of fluid in a circular tube/micro-capillary obeying the Meter model is given as:

$$Q = -\frac{dP}{dx}\frac{\pi\,R^4}{8\,\eta_0\,\eta_\infty}\Bigg((\eta_\infty-\eta_0)_3\mathrm{F}_2\left(1,\frac{2}{S},\frac{4}{S};\frac{S+2}{S},\frac{S+4}{S};-\frac{\eta_\infty}{\eta_0}\left(-\frac{dP}{dx}\frac{R}{2\,\tau_{\mathrm{m}}}\right)^S\right)+2\,(\eta_0-\eta_\infty)_2\mathrm{F}_1\left(1,\frac{2}{S};\frac{S+2}{S};-\frac{\eta_\infty}{\eta_0}\left(-\frac{dP}{dx}\frac{R}{2\,\tau_{\mathrm{m}}}\right)^S\right)-\eta_0\Bigg), \tag{16}$$

here, the hypergeometric function ${}_2F_1(a,b;c;z)$ is defined as in Eq. 17 and the hypergeometric function ${}_3F_2(a,b,c;d,e;z)$ is defined as in Eq. 18:

$${}_2F_1(a,b;c;z) = \sum_{n=1}^{\infty}\frac{(a)_n\,(b)_n\,z^n}{(c)_n\,n!}, \tag{17}$$

$${}_3F_2(a,b,c;d,e;z) = \sum_{n=1}^{\infty}\frac{(a)_n\,(b)_n\,(c)_n\,z^n}{(d)_n\,(e)_n\,n!}, \tag{18}$$

The `hypergeom` function of MATLAB was used to solve a generalized hypergeometric function of the analytical solution of the Meter model. The generalized hypergeometric functions ${}_2F_1(a,b;c;z)$ and ${}_3F_2(a,b,c;d,e;z)$ are series as given in the Eq. S6 and S7 of SI, respectively, which converge for $|z|<1$. Since, all parameters of hypergeometric function of the Meter model are constant values, the series of the generalized hypergeometric function of the Meter model can be solved using `hypergeom` function of MATLAB without error over a range of pressure gradient, radius, and Meter model parameters.

Section S2 of the SI illustrates that the MM converts to existing shear stress-dependent rheological models (i.e., Reiner–Philippoff model (Reiner 1930; Philippoff 1935), Ellis model (Matsuhisa and Bird 1965)). The analytical solution for Newtonian fluid and Reiner–Philippoff model fluid can be derived using the analytical solution of the MM (see Section S2 of the SI).

Section S2.1 of the SI shows that Eq. 12 and Eq. 16 convert to Hagen–Poiseuille equation on substituting $\eta_0 = \eta_\infty$. On equating Eq. 16 with the Hagen–Poiseuille equation ($Q = \frac{\pi R^4}{8\eta}\frac{dP}{dx}$) and substituting $\frac{dP}{dx}\frac{R}{2} = \tau_{\mathrm{w}}$ in Eq. 16, we obtain an equation for an effective viscosity (η_{eff}) of fluid in terms of wall shear stress (τ_{w}) as follows:

$$\frac{1}{\eta_{\mathrm{eff}}} = \frac{1}{\eta_0\,\eta_\infty}\Bigg((\eta_\infty-\eta_0)_3\mathrm{F}_2\left(1,\frac{2}{S},\frac{4}{S};\frac{S+2}{S},\frac{S+4}{S};-\frac{\eta_\infty}{\eta_0}\left(\frac{\tau_{\mathrm{w}}}{\tau_{\mathrm{m}}}\right)^S\right)+2\,(\eta_0-\eta_\infty)_2\mathrm{F}_1\left(1,\frac{2}{S};\frac{S+2}{S};-\frac{\eta_\infty}{\eta_0}\left(\frac{\tau_{\mathrm{w}}}{\tau_{\mathrm{m}}}\right)^S\right)-\eta_0\Bigg), \tag{19}$$

Equation 19 helps determine the effective viscosity (η_{eff}) of a non-Newtonian fluid from measurable parameters η_0, η_∞, τ_{m}, S, τ_{w}, R, and $\frac{dP}{dx}$. On comparing Eq. 16 with Darcy's law ($Q_{\mathrm{darcy}} = \frac{k\,A}{\eta}\frac{dP}{dx}$), we obtain an effective viscosity value as given in Eq. 19 and permeability (k) of the porous media as ($k = \frac{r_{\mathrm{eff}}^2}{8}$). Here, r_{eff} is the hydraulic radius of porous medium. Thus, the effective viscosity determined using Eq. 19 could be advantageous in determining Darcy scale flow rate and velocity of a non-Newtonian fluid in a porous medium.

We observed that the effective viscosity value obtained using Eq. 19 consistently appears at a distance of ($0.8R$) from the center of a capillary for all experimental flow data utilized in present work. This suggests that the value of effective viscosity is equal to the viscosity value at a distance of $\beta\,R$ from the center of the tube, where $0<\beta<1$. Thus, the approximate effective viscosity of the MM fluid for a given flow condition will be as in Eq. 20:

$$\eta_{\mathrm{eff}} = \eta_\infty + \frac{\eta_0-\eta_\infty}{1+\left(\frac{\beta\,R}{2\,\tau_{\mathrm{m}}}\frac{dP}{dx}\right)^S} \tag{20}$$

Here, $\beta = 0.8$ for flow through a circular geometry. We note that different geometric shapes will have different β value. Equation 20 is an easy-to-use equation for estimation of the effective viscosity of the fluid for a given fluid flow condition compared to Eq. 19. The advanced mathematical tool is required to estimate effective viscosity value using Eq. 19 due to the presence of hypergeometric function in the equation. We obtain a semi-analytical solution for the flow rate of MM fluid by substituting Eq. 20 in Hagen–Poiseuille equation as:

$$Q = \frac{dP}{dx}\frac{\pi R^4}{8\left(\eta_\infty + \dfrac{\eta_0 - \eta_\infty}{1 + \left(\dfrac{\beta R}{2\tau_m}\dfrac{dP}{dx}\right)^S}\right)} \tag{21}$$

We define the effective Reynolds number (Re_{eff}) of MM fluid as:

$$Re_{eff} = \frac{2\rho U_{avg} R}{\eta_{eff}} \tag{22}$$

The Darcy friction factor (f_D) during any type of a fluid flow is $f_D = \frac{dP}{dx}\frac{4R}{\rho U_{avg}^2}$. We obtain effective friction factor (f_{eff}) for laminar flow of MM fluid (Eq. 23) by substituting the MM analytical solution for average velocity (Eq. 15) in Darcy's friction factor equation.

$$f_{eff} = \frac{256}{\rho R^3 \left(\frac{dP}{dx}\right)}\eta_{eff}^2 = \frac{128}{\rho R^2 \tau_w}\eta_{eff}^2 \tag{23}$$

Results and discussion

Meter model for shear-thinning and shear-thickening fluids

Figure 1 shows a statistically good fit of experimental and MM predicted (Eq. 2) viscosity–shear stress and shear rate–shear stress data of a shear-thinning fluid (xanthan gum fluid of Campagnolo et al. (2013) over a range of concentrations, polyacrylamide (PAA) fluid of Escudier et al. (2005)) and shear-thickening fluid (cornstarch fluid in glycerol-water mixture of Brown and Jaeger (2012)). The model parameters are estimated using Excel-Solver methods that use GRG nonlinear algorithm (Kemmer and Keller 2010). Figure 1 shows that cornstarch fluid has a shear-thinning region at lower shear stresses and high shear stresses. Literature reports a similar behavior for most of shear-thickening fluids; thus, an application of MM for shear-thickening fluids should be restricted to the shear-thickening region of the viscosity–shear stress curve.

The material parameters of MM (Table 1) imply that the zero shear viscosity (η_0) and critical shear stress (τ_m) increase exponentially and the shear-thinning property of xanthan gum fluid (i.e., exponent S) increases linearly with an increase in the concentration of the xanthan gum fluid. This implies that MM helps quantitatively correlate effect of physico-chemical parameters (e.g., XG concentration in the present case) on rheology of shear-thinning and shear-thickening fluids using measurable parameters.

The factor β

To determine β over a range of pressure gradient, radius and Meter model parameter, we substitute Eq. 20 in Eq. 19 and solved resultant equation for β. Figure 2 shows that the factor β values ranged from 0.73 to 0.82 over a range a pressure-gradient, radius, and Meter model parameters. The average value of the $\beta = 0.8$ suggests that an effective viscosity of the fluid measured at a distance $0.8R$ distance from the centre of the capillary can be considered an approximate effective viscosity of the fluid.

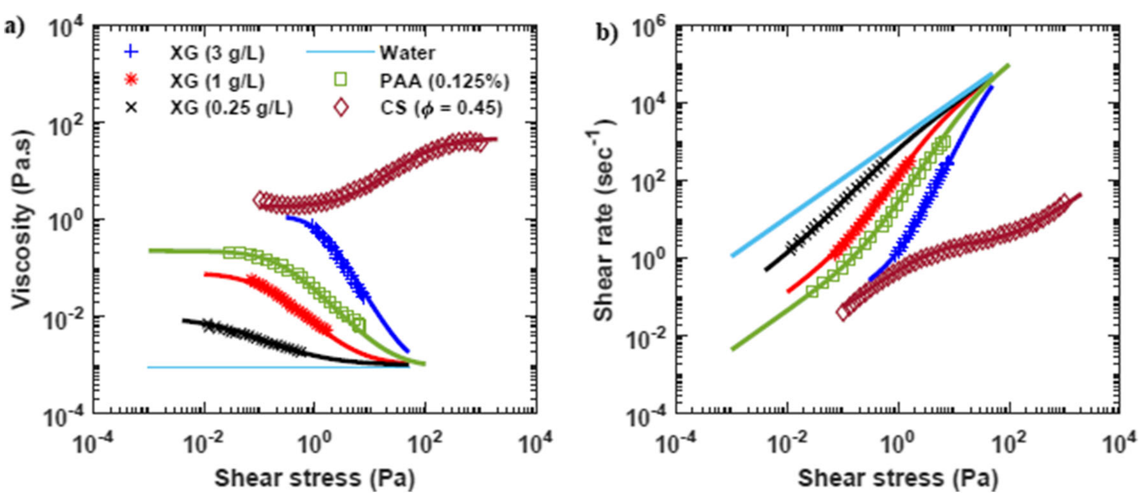

Fig. 1 **a** Shear viscosity as a function of shear stress (Eq. 2); **b** shear rate as a function of shear stress (Eq. 4) modelled using MM. An experimental rheological data of xanthan gum (XG) fluid over a range of concentrations (3 g/L, 1 g/L, 0.25 g/L, water) (Campagnolo et al. 2013); 0.125% polyacrylamide (PAA) fluid (Escudier et al. 2005), cornstarch (CS) fluid having volume fraction of 0.45 (Brown and Jaeger 2012) modelled using MM. Continuous line shows MM predications. The material parameters of MM are given in Table 1. The root means square error (RMSE) ranges from 3.4×10^{-3} to 1.6×10^{-1}

Table 1 MM parameters of Campagnolo et al. (2013), Escudier et al. (2005), and Brown and Jaeger (2012)

Parameter	Shear-thinning fluid					Shear-thickening fluid
	Xanthan gum (XG) concentration (g/L)				PAA	Cornstarch (CS)
	(Campagnolo et al. 2013)				(Escudier et al. 2005)	(Brown and Jaeger 2012)
	3 g/L	1 g/L	0.25 g/L	0	0.125%	$\phi = 0.45$
η_0 (Pa·s)	1.2	0.08	0.01	0.000896	0.2257	1.8
η_∞ (Pa·s)	0.000896	0.000896	0.000896	0.000896	0.000896	46
τ_m (Pa)	1.1	0.105	0.028	1	0.24	100
S	1.87	1.11	0.75	1	1.124	1.1
λ [s]	0.546	0.385	0.195		0.47	0.24

Validation of the analytical solution of the Meter model

(a) Flow through a micro-capillary

An experimental velocity profile of Campagnolo et al. (2013) gave good fit with the analytical solution of the MM for radial velocity profile (Eq. 12) at the pressure gradients of 92,000 Pa/m, 16,500 Pa/m, 4900 Pa/m, and 2000 Pa/m during flow of 3 g/L, 1 g/L, and 0.25 g/L xanthan gum fluid and water (0.4% milk), respectively (see Fig. 3a). Moreover, the analytical (Eq. 16) and semi-analytical (Eq. 21) solutions of the MM for flow rate could correctly determine the experimental flow rate of 30 µL/min through a circular microfluidic channel of radius 160 µm. Figure 3b suggests that the viscosity profile of the non-Newtonian shear-thinning fluid is bell-shaped in a circular geometry. The viscosity increases gradually near the wall and drastically in the central region of the micro-capillary. The effective viscosity estimated using Eq. 19 and Eq. 20 for flow of a 3 g/L, 1 g/L, and 0.25 g/L xanthan gum fluid through a micro-capillary is 0.041 Pa·s, 0.0075 Pa·s, and 0.0022 Pa·s, respectively. We note that the analytical solution of the Meter model fluids is applicable for shear-thickening fluid and needs validation using experimental data.

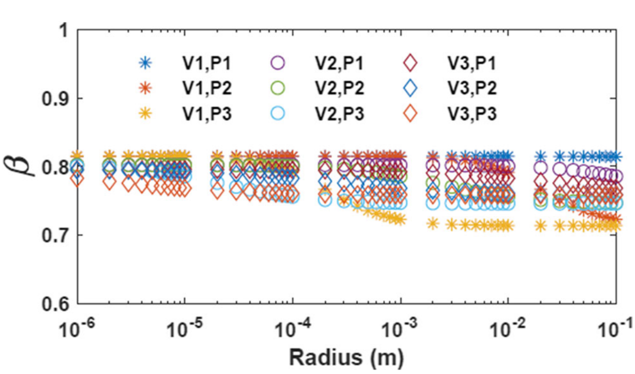

Fig. 2 The factor β over a range of a pressure gradient, radius, and Meter model parameters. V1, V2, and V3 represent viscosity of the 3g/L, 1 g/L, and 0.25 g/L xanthan gum fluid, respectively, as given in Table 1. P1 = 10^2 Pa/m, P2=10^4 Pa/m, and P3 = 10^6 Pa/m

(b) Flow through a tube

Escudier et al. (2005) measured radial velocity profile of 0.125% polyacrylamide (PAA) fluid flow in a circular tube (radius 5 cm) over a range of Reynolds number (Re_{expt}), wherein the authors defined Reynolds number (Re_{expt}) using shear viscosity at the wall of pipe. Figure 4a depicts that the analytical solution of the MM for the velocity profile (Eq. 12) could correctly predict the experimentally observed radial velocity profile at $Re_{\mathrm{expt}} = 676$ and $Re_{\mathrm{expt}} = 1620$. The analytical solution of MM is restricted to laminar flow and Fig. 4a suggests that at $Re_{\mathrm{expt}} = 5020$ PAA flow is in transition phase and at $Re_{\mathrm{expt}} = 42900$ is in turbulent phase. Figure 4b shows that the shape of the viscosity profile becomes more acute at the center of the circular tube with an increase in Reynolds number or pressure gradient.

The effective Reynolds number (Re_{eff}) values calculated using Eq. 22 are drastically different from Re_{expt} estimated by Escudier et al. (2005) (see Table 2). The analytical solution of the MM could correctly estimate the velocity profile, flow rate, average velocity, and friction factor within the error range (± 5%), when Re_{eff} of PAA is less than 1241 (at $\frac{dP}{dx} < 51$ Pa/m). On the contrary, when Re_{eff} was 3178 (at $\frac{dP}{dx} = 70$ Pa/m) and 14,007 (at $\frac{dP}{dx} = 109$ Pa/m), flow becomes turbulent, and velocity profile could not be matched with the experimental data. This result suggests that the Reynolds number determined using Eq. 22 gives comparable results with the Reynolds number of a Newtonian fluid in a circular tube. Thus, it is convenient to define a non-Newtonian fluid flow as (i) laminar if $Re_{\mathrm{eff}} < 2300$, (ii) turbulent if $Re_{\mathrm{eff}} > 2900$, and (iii) transition zone if $2300 < Re_{\mathrm{eff}} < 2900$.

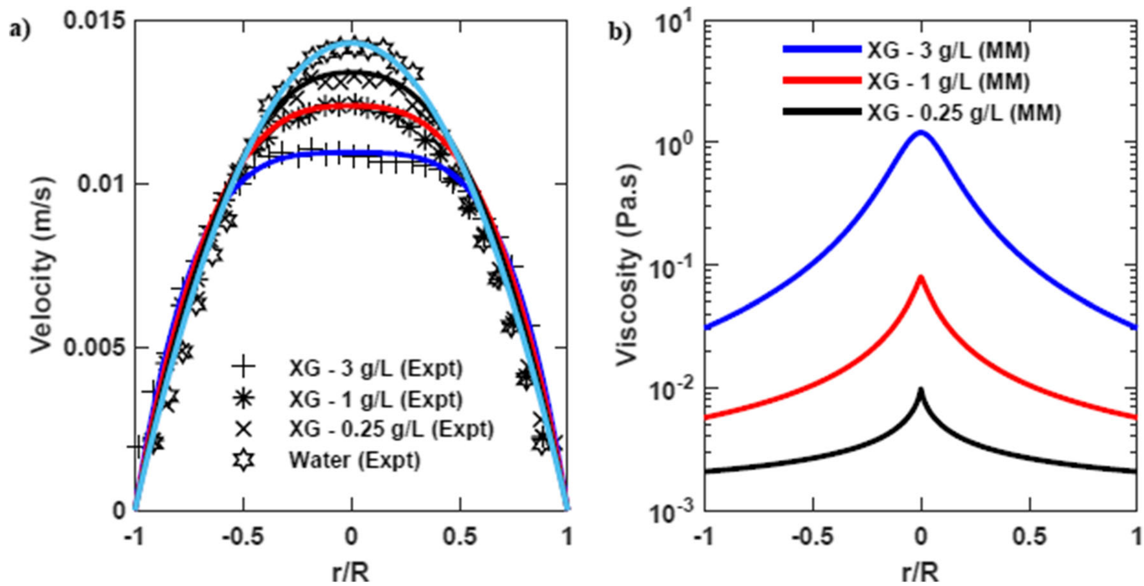

Fig. 3 Comparison of experimental (Campagnolo et al. 2013) and MM analytical solution predicated by Eq. 12, **a** radial velocity profile, and **b** radial viscosity profile during flow of a xanthan gum (XG) through a circular micro-capillary (radius 160 μm) over a range of XG concentrations.The material parameters of MM are given in Table 1. The root means square error (RMSE) ranges from 3.4×10^{-4} to 6.3×10^{-2}

As given in Table 2, the friction factor of the MM determined using Eq. 23 and the experimental friction factor (f_D) determined using Darcy's law give approximately the same result for a laminar flow (Re_{eff} < 1241). As expected for the turbulent flow, the friction factor estimate has a difference of 26% at $\frac{dP}{dx} = 70$ Pa/m and 142% at $\frac{dP}{dx} = 109$ Pa/m. For a Newtonian fluid, the relationship between the Reynolds number and the friction factor for laminar flow through a circular tube is given as $Re = \frac{64}{f_D}$. The same relationship applies to non-Newtonian fluid described by the MM. The Re_{eff} estimated using Eq. 22 is equivalent to the

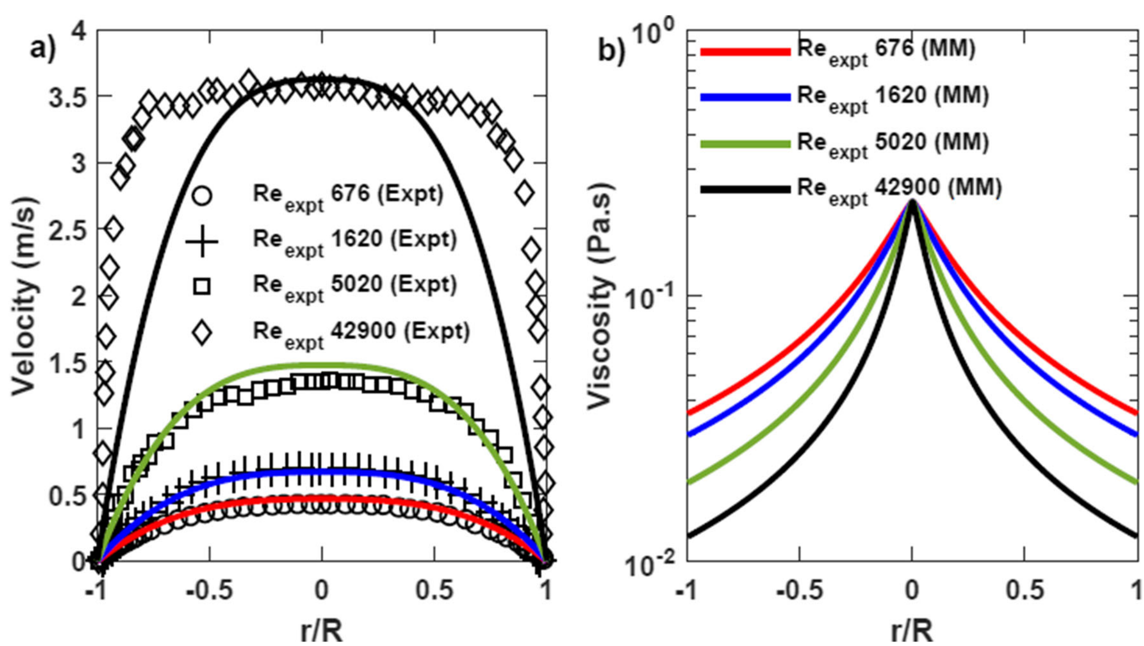

Fig. 4 Comparison of experimental (Escudier et al. 2005) and MM analytical solution predicated by Eq. 12, **a** radial velocity profile, and **b** radial viscosity profile during flow of a 0.125% polyacrylamide (PAA) fluid through a circular micro-capillary (radius 0.05 m) over a range of Reynolds numbers. The material parameters of MM are given in Table 1. The root means square error (RMSE) ranges from 3.4×10^{-4} to 8.5×10^{-3} for $Re_{\mathrm{expt}} < 1620$

Table 2 Validation of the analytical solution of MM for flow through a circular tube

Experimental observation (Escudier et al. 2005)					MM estimate				
Re_{expt}	$\frac{dP}{dx}$	U_{expt}	η_{w}	f_{D}	η_{eff}	Q	U_{Avg}	Re_{eff}	f_{eff}
	(Pa/m)	(m/s)	(Pa·s)		(Pa·s)	(m^3/s)	(m/s)		
676	38.5	0.256	0.0376	0.1135	0.0467	0.002	0.2578	552	0.1158
1620	51	0.447	0.0276	0.0510	0.0358	0.0035	0.448	1241	0.0516
5020	70	0.939	0.0187	0.0159	0.0262	0.0065	0.8339	3178	0.0201
42900	109	3.36	0.0078	0.0019	0.0156	0.0172	2.184	14007	0.0046

Reynolds number estimated using $Re_{\text{eff}} = \frac{64}{f_{\text{D}}}$, if an experimental error of up to 5% is taken into account for laminar flow of Escudier et al. (2005).

The effective friction factor

A simple algebraic formula for the effective friction factor as a function of pressure gradient, radius, and Meter model parameters (η_∞, η_0, τ_{m}, S), as presented in Eq. 24, can be obtained on substituting Eq. 20 in Eq. 23. This is a semi-analytical formula for the effective friction factor of the Meter model fluid.

$$f_{\text{eff}} = \frac{256}{\rho\, R^3 \left(\frac{dP}{dx}\right)} \left(\eta_\infty + \frac{\eta_0 - \eta_\infty}{1 + \left(\frac{0.8\, R}{2\, \tau_{\text{m}}} \frac{dP}{dx} \right)^S} \right)^2 \tag{24}$$

Figure 5 shows that the effective friction factor estimated using Eq. 23 closely matches the f_{eff} estimated using Eq. 24 over a range of xanthan gum concentrations. Figure 5 also shows a non-linear relationship between the pressure gradient and the effective friction factor. An increase in the radius of the circular capillary/pipe decreases the friction factor. Moreover, increase in the polymeric concentration of xanthan gum fluid shows increase in f_{eff} over a range of pressure gradients and radii. The results suggest that Eq. 24 can be utilized to determine f_{eff} of a non-Newtonian fluid using measurable parameters (i.e., radius, pressure gradient, and Meter model parameters).

Radial viscosity variation

We determined radial viscosity variation (%) during flow of an MM fluid through a circular tube/micro-capillary using Eq. 25.

$$\text{Radial viscosity variation (\%)} = \frac{(\eta_{\text{center}} - \eta_{\text{w}})}{\eta_{\text{center}}} \times 100, \tag{25}$$

here, η_{center} and η_{w} are the viscosity at the center and wall of a circular tube, respectively. The variation of viscosity along the radial direction in a circular tube/capillary depends on radius and pressure gradient, i.e., on shear stress. Figure 6a shows estimated radial viscosity variation (%) at various pressure gradients (1 to 10^8 Pa/m) and a radius (0.05 µm–500 mm) during XG-3 g/L fluid flow of Campagnolo et al. (2013) in a circular tube/capillary. Similarly, Fig. 6b elucidates radial viscosity variation (%) at various Reynolds numbers (10^{-9} to 10^7) and pressure gradients (10^{-1} to 10^6 Pa/m).

It appears from Fig. 6a that for each radius, there exists a critical pressure gradient value below which the viscosity variation is insignificant. If radial viscosity variation of 10^{-1}% is considered an insignificant variation, then 10^6 Pa/m, 10^5 Pa/m, 10^4 Pa/m, 10^3 Pa/m, 10^2 Pa/m, and 10^1 Pa/m will be the critical/threshold pressure gradient values for capillaries of radius 0.05 µm, 0.5 µm, 5 µm, 50 µm, 500 µm, and 5 mm, respectively. Below these thresholds, the viscosity variation could be considered as insignificant or effectively constant. The choice of viscosity variation as "an insignificant" might depend on the viscosity at a zero shear stress (η_0), and effect of the viscosity variation on the output of work. Figure 6a also suggests that with an increase in the radius of a capillary, magnitude of the critical pressure gradient decreases.

Similarly, Fig. 6b shows that, for each pressure gradient, there exists a critical Reynolds number below which the viscosity variation is insignificant. Figure 6b shows that if pressure gradient of the XG-3 g/L fluid through a circular tube/micro-capillary is lower than 100 Pa/m and Reynolds number is below 0.001, the radial viscosity variation is insignificant. Overall, Fig. 6 illustrates that if applied pressure gradients or Reynolds numbers are below their threshold/critical values, the non-Newtonian fluid flow can be modelled as a Newtonian fluid with zero shear stress viscosity as its constant viscosity. This means that the fluid flow through capillary can be modelled using the Hagen–Poiseuille equation.

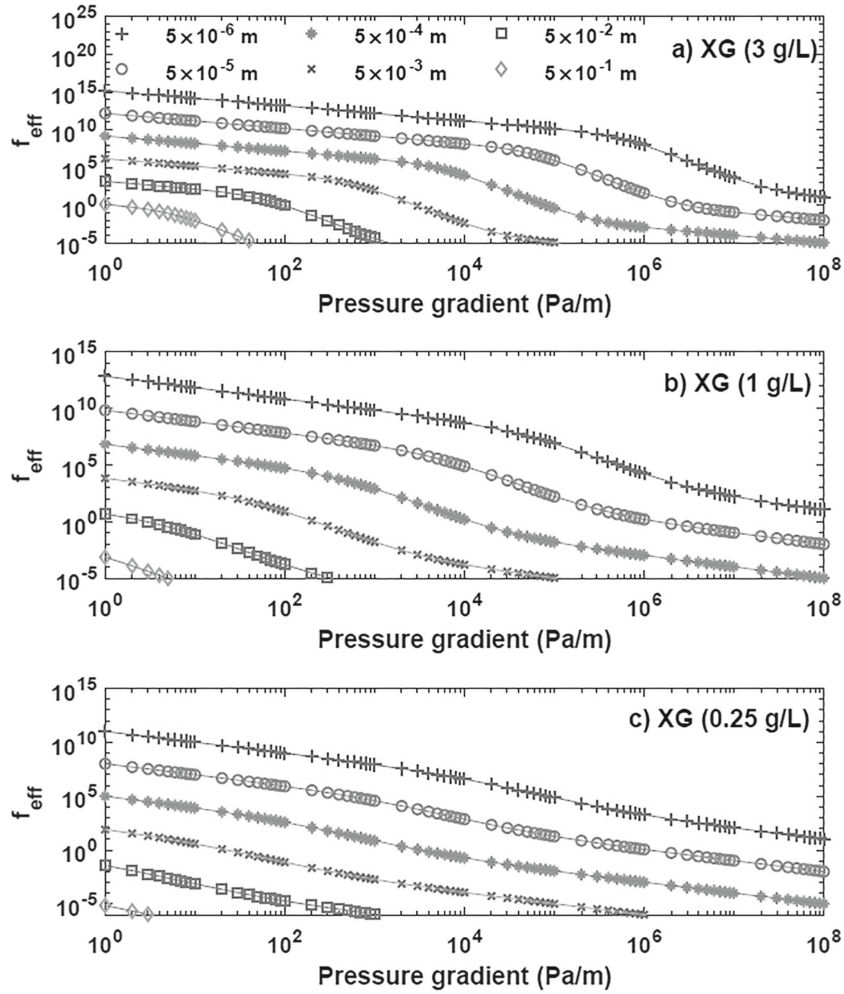

Fig. 5 The effective friction factor as a function of pressure gradient over a range of radii (5 µm to 0.5 m) and xanthan gum (XG) concentrations. **a** XG 3 g/L; **b** XG 1 g/L; and **c** XG 0.25 g/L. Symbols show f_{eff} estimated using Eq. 23 and continuous solid lines show f_{eff} estimated using Eq. 24 for radius (R) of capillary/tube. Meter model parameters are given in Table 1

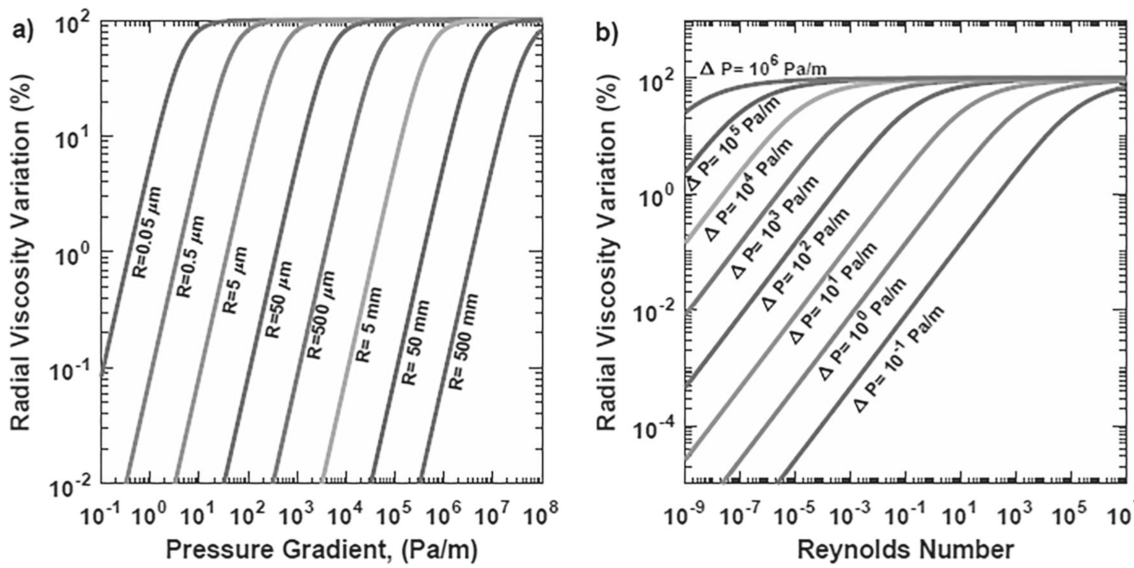

Fig. 6 **a** Effect of pressure gradient and radius (R) on the radial viscosity variation (%) during flow of a xanthan gum (XG, 3 g/L) fluid of Campagnolo et al. (2013) in a circular capillary/tube, **b** effect of Reynolds number and pressure gradient on the radial viscosity variation (%) during flow of a xanthan gum (XG, 3 g/L) fluid of Campagnolo et al. (2013) in a circular capillary/tube

Conclusions

The Meter model was validated against experimental rheological data of cornstarch fluid, polyacrylamide fluid, and xanthan gum fluid. The analytical solution of the MM was validated against the experimentally measured velocity profile during flow of non-Newtonian fluids (xanthan gum and polyacrylamide) through a circular micro-capillary of radius 160 μm and a circular tube of radius 0.05 m. An easy to use semi-analytical solution (similar to Hagen–Posseuille equation) is formulated for computation of an effective viscosity and a flow rate. The effective Reynolds number estimated using formulation presented in this work helps to correctly characterize fluid flow in laminar, turbulent, and transition flows. The Darcy friction factor computed using formulation given in the current work, and experimental friction factor gave equivalent results for laminar flow. Finally, this work suggested that there exists a threshold pressure gradient for a given radius and a critical effective Reynolds number below which the radial viscosity variation is insignificant, and it will be convenient to assume a constant viscosity for such flows.

The method proposed in the present work to compute effective viscosity, average velocity, radial velocity profile, flow rate, effective Reynolds number, and effective friction factor using measurable flow parameters will help in understanding the behavior of non-Newtonian fluids comprehensively. In the future, we will apply the proposed model for the flow of non-Newtonian fluids in heterogeneous porous media using OpenFOAM and pore-network model and compare our results to similar recent publications, for example, Zami-Pierre et al. (2018).

Supporting Information

The SI includes:

- Time-independent non-Newtonian fluid empirical models (Table S1);
- Analytical solution for existing rheological models (Section S2);
- The generalized hypergeometric function (Section S3)

Acknowledgments T.S. gratefully appreciates Rajashri Shahu Maharaj Foreign Scholarship, Government of Maharashtra, India, that has enabled him to undertake PhD research at the University of Manchester.

Compliance with ethical standards

Conflict of interest The authors declare that they have no conflict of interest.

References

Balhoff MT, Thompson KE (2006) A macroscopic model for shear-thinning flow in packed beds based on network modeling. Chem Eng Sci 61(2):698–719

Bird RB, Armstrong RC, Hassager O (1987) Fluid mechanics, dynamics of polymeric liquids, Vol. 1, Wiley, New York

Bird RB, Carreau PJ (1968) A nonlinear viscoelastic model for polymer solutions and melts—I. Chem Eng Sci 23(5):427–434

Bird RB, Stewart WE, Lightfoot EN (2007) Transport phenomena. John Wiley & Sons, Hoboken

Brown E, Jaeger HM (2012) The role of dilation and confining stresses in shear thickening of dense suspensions. J Rheol 56(4):875–923

Campagnolo L, Nikolić M, Perchoux J, Lim YL, Bertling K, Loubiere K, Prat L, Rakić AD, Bosch T (2013) Flow profile measurement in microchannel using the optical feedback interferometry sensing technique. Microfluid Nanofluid 14(1-2):113–119

Cross MM (1965) Rheology of non-Newtonian fluids: a new flow equation for pseudoplastic systems. J Colloid Sci 20(5):417–437

Duda JL, Hong SA, Klaus EE (1983) Flow of polymer solutions in porous media: inadequacy of the capillary model. Industrial & Engineering Chemistry Fundamentals 22(3):299–305

Eberhard U, Seybold HJ, Floriancic M, Bertsch P, Jiménez-Martínez J, Andrade Jr JS, Holzner M (2019) Determination of the effective viscosity of non-Newtonian fluids flowing through porous media. Frontiers in Physics 7:71

Escudier MP, Poole RJ, Presti F, Dales C, Nouar C, Desaubry C, Graham L, Pullum L (2005) Observations of asymmetrical flow behaviour in transitional pipe flow of yield-stress and other shear-thinning liquids. J Non-Newtonian Fluid Mech 127(2-3):143–155

Ferrás LL, Afonso AM, Alves MA, Nóbrega JM, Pinho FT (2020) Newtonian and viscoelastic fluid flows through an abrupt 1: 4 expansion with slip boundary conditions. Phys Fluids 32(4):043103

Kemmer G, Keller S (2010) Nonlinear least-squares data fitting in Excel spreadsheets. Nature protocols 5(2):267

Kim SK (2018) Flow-rate based method for velocity of fully developed laminar flow in tubes. J Rheol 62(6):1397–1407

Matsuhisa S, Bird RB (1965) Analytical and numerical solutions for laminar flow of the non-Newtonian Ellis fluid. AIChE J 11(4):588–595

Meter DM (1964) Tube flow of non-Newtonian polymer solutions: Part II. turbulent flow. AIChE J 10(6):881–884

Meter DM, Bird RB (1964) Tube flow of non-Newtonian polymer solutions: part I. Laminar flow and rheological models. AIChE J 10(6):878–881

Metzner AB, Reed JC (1955) Flow of non-Newtonian fluids—correlation of the laminar, transition, and turbulent-flow regions. AlChe Journal 1(4):434–440

Peralta JM, Meza BE, Zorrilla SE (2014) Mathematical modeling of a dip-coating process using a generalized Newtonian fluid. 1. Model development. Industrial & Engineering Chemistry Research 53(15):6521–6532

Peralta JM, Meza BE, Zorrilla SE (2017) Analytical solutions for the free-draining flow of a Carreau-Yasuda fluid on a vertical plate. Chem Eng Sci 168:391–402

Peters GWM, Schoonen JFM, Baaijens FPT, Meijer HEH (1999) On the performance of enhanced constitutive models for polymer melts in a cross-slot flow. J Non-Newtonian Fluid Mech 82(2-3):387–427

Philippoff W (1935) Zur Theorie der Strukturviskositaet. I. Kolloid-Zeitschrift 71(1):1–16

Reiner M (1930) In search for a general law of the flow of matter. Journal of Rheology (1929-1932) 1(3):250–260

Sadowski TJ, Bird RB (1965) Non-Newtonian flow through porous media. I. Theoretical. Transactions of the Society of Rheology 9(2):243–250

Savins JG (1969) Non-Newtonian flow through porous media. Industrial & Engineering Chemistry 61(10):18–47

Sochi T (2015) Analytical solutions for the flow of Carreau and Cross fluids in circular pipes and thin slits. Rheol Acta 54(8):745–756

Sochi T, Blunt MJ (2008) Pore-scale network modeling of Ellis and Herschel–Bulkley fluids. J Pet Sci Eng 60(2):105–124

Steller R, Iwko J (2018) New generalized Newtonian fluid models for quantitative description of complex viscous behavior in shear flows. Polymer Engineering & Science 58(8):1446–1455

Tsakiroglou CD, Theodoropoulou M, Karoutsos V, Papanicolaou D, Sygouni V (2003) Experimental study of the immiscible displacement of shear-thinning fluids in pore networks. J Colloid Interface Sci 267(1):217–232

Tsakiroglou C, Theodoropoulou M, Karoutsos V (2003) Fluid flow in fractured formations. In: New paradigms in subsurface prediction, Springer, pp 161–172

Tsakiroglou CD (2002) A methodology for the derivation of non-Darcian models for the flow of generalized Newtonian fluids in porous media. J Non-Newtonian Fluid Mech 105(2-3):79–110

Yasuda K (1979) Investigation of the analogies between viscometric and linear viscoelastic properties of polystyrene fluids. Ph.D. Thesis, Massachusetts Institute of Technology

Yilmaz F, Gundogdu MY (2008) A critical review on blood flow in large arteries; relevance to blood rheology, viscosity models, and physiologic conditions. Korea-Australia Rheology Journal 20(4):197–211

Zami-Pierre F, de Loubens R, Quintard M, Davit Y (2018) Effect of disorder in the pore-scale structure on the flow of shear-thinning fluids through porous media. J Non-Newtonian Fluid Mech 261:99–110